EPJ Web of Conferences **377**, 06008 (2026) https://doi.org/10.1051/epjconf/202637706008
IPS 2026

Physics-Based 3D Simulation with Real-Time Extraction of Wave Parameters from Spatiotemporal Data

Dwi Susanti[1*], *Slamet* Maulana[2], *Fahmi* Fatkhomi[3], *Elvara Norma* Aroyandini[4], and *Nikki Faith Alburo* Bantillo[5]

[1]Physics Education Program Study, Faculty of Mathematics and Natural Science, Universitas Negeri Jakarta, Jakarta, Indonesia
[2]Labschool Cibubur Senior High School, Jl. Raya Hankam Kampus Labschool No. 15-20, Bekasi 17432, West Java, Indonesia
[3]Universitas Pancasakti Tegal, Indonesia
[4]Primary School Teacher Education Program Study, Faculty of Islamic Education and Teacher Training, Universitas Alma Ata, Bantul, Indonesia
[5]Dr. Emilio B. Espinosa Sr. Memorial State College of Agriculture and Technology, Philippines

Abstract. Wave simulation has become a vital approach for studying dynamic propagation phenomena, representing temporal and spatial evolution simultaneously. Existing simulation platforms predominantly emphasize visual representation and conceptual demonstration, while the quantitative extraction of wave parameters remains separated from the simulation environment. Consequently, there is a lack of integration between physics-based simulation, spatiotemporal sampling, and real-time parameter extraction. This study proposes a physics-based 3D simulation framework capable of extracting frequency, wavelength, and amplitude directly from dynamically generated spatiotemporal wave data in real time. We utilize the 3D scalar wave equation, coupled with discrete spatial and temporal sampling mechanisms, to generate propagating waves. A real-time algorithm employing peak detection and zero-crossing analysis continuously acquires parameter values. Experimental scenarios covering frequency (1-10 Hz) and amplitude (0.1-1 m) variations demonstrate the system's high precision. Validation against analytical solutions reveals a Mean Absolute Percentage Error (MAPE) of less than 1.5% and a Root Mean Square Error (RMSE) below 0.02, while sustaining an operation rate of 60 frames per second. These results confirm that wave parameters can be extracted automatically and accurately, preserving physical consistency without compromising real-time computational performance, offering a robust tool for advanced computational physics education and extensive future multidisciplinary applied physical studies.

* Corresponding author: dwisusanti@unj.ac.id

1 Introduction

Wave simulation has become an important approach for studying dynamic propagation phenomena due to its ability to represent temporal and spatial evolution simultaneously [1]. In computational physics, visualizing complex three-dimensional (3D) wave dynamics is essential to understanding phenomena spanning acoustic, electromagnetic, and mechanical domains [2, 3]. Implementing numerical models allows researchers and students to observe physical properties like interference and diffraction directly on screen, providing an intuitive understanding that is difficult to capture through static mathematical models alone.

However, existing simulation platforms predominantly emphasize visual representation and conceptual demonstration while quantitative extraction of wave parameters remains separated from the simulation environment [4]. In conventional educational and research tools, visual outputs are highly refined, yet the underlying wave properties must often be calculated manually using external software after the data has been exported [5]. This manual pipeline creates a disconnect between the observation of the simulation and the quantitative analysis of the position-time data, restricting dynamic, on-the-fly learning and experimentation [6].

Consequently, a significant scientific gap persists regarding the integration of a rigorous physics-based simulation with dynamic spatiotemporal sampling and real-time parameter extraction within a unified framework [7]. Most existing methodologies either compromise numerical fidelity to achieve interactive frame rates or sacrifice real-time feedback for the sake of high-precision mathematical extraction [8]. The lack of an embedded, automatic measurement system capable of operating directly on simulated 3D spatial grids limits the depth of real-time analysis achievable in standard desktop simulation environments [9].

This study proposes a physics-based 3D simulation framework capable of extracting frequency, wavelength, and amplitude directly from dynamically generated spatiotemporal wave data in real time. The primary contributions of this work are fourfold (1) the development of a 3D physics-based simulation utilizing explicit finite difference methods; (2) the design of an automatic signal extraction algorithm based on spatiotemporal peak detection and zero-crossing mechanics; (3) the facilitation of quantitative measurement simultaneously with 3D visualization; and (4) the validation of the extracted simulation data against established analytical wave solutions to ensure high computational fidelity.

This study proposes a physics-based 3D simulation framework capable of extracting frequency, wavelength, and amplitude directly from dynamically generated spatiotemporal wave data in real time. The primary contributions of this work are fourfold [1] the development of a 3D physics-based simulation utilizing explicit finite difference methods; [2] the design of an automatic signal extraction algorithm based on spatiotemporal peak detection and zero-crossing mechanics; [3] the facilitation of quantitative measurement simultaneously with 3D visualization; and [4] the validation of the extracted simulation data against established analytical wave solutions to ensure high computational fidelity.

2 Theoretical Background

2.1 Wave Representation

The fundamental behavior of a harmonic wave propagating through a three-dimensional medium is described by the scalar wave equation. The analytical solution for displacement Ψat a given spatial position $\mathrm{r} = (x, y, z)$and time t is expressed as

$$\Psi(\mathrm{r}, t) = A \sin(\mathrm{k} \cdot \mathrm{r} - \omega t + \phi) \quad (1)$$

Where A is the maximum amplitude of the wave, representing the peak displacement from equilibrium. The angular frequency ω dictates the rate of oscillation in the temporal domain, while the wave vector k defines the spatial frequency and the direction of wave propagation.

2.2 Parameter Relationship

The physical consistency of any wave simulation relies heavily on the strict interplay between the extracted parameters. The fundamental relationships are governed by The fundamental relationships are governed by the following standard formulas [10]

$$\omega = 2\pi f \tag{2}$$

$$k = \frac{2\pi}{\lambda} \tag{3}$$

$$v = \lambda f \tag{4}$$

Where v is the phase velocity of the wave, f is the temporal frequency, and λ is the spatial wavelength. Frequency extraction involves monitoring a single point in space over time to measure the period $T = \frac{1}{f}$. Conversely, wavelength extraction requires freezing time and analyzing the spatial distance between consecutive in-phase points (peak-to-peak).

2.3 Spatiotemporal Signal Representation

To bridge continuous physics with computational models, the continuous wave function $\Psi(\mathrm{r}, t)$must be mapped to a discrete space. The spatiotemporal signal representation is defined as

$$\Psi_{i,j,k}^{n} = \Psi(i\Delta x, j\Delta y, k\Delta z, n\Delta t) \tag{5}$$

$\Delta x, \Delta y, \Delta z$ represent the spatial discretization steps (spatial sampling), and Δt represents the time step (temporal sampling). The accuracy of real-time extraction algorithms depends significantly on the resolution of these sampling intervals to avoid aliasing artifacts.

3 Computational Method

3.1 Physics-Based Simulation Engine

The core of the simulation is driven by the 3D scalar wave equation

$$\frac{\partial^2 \Psi}{\partial t^2} = v^2 \nabla^2 \Psi \tag{6}$$

The employed an explicit Finite Difference Time Domain (FDTD) scheme to discretize the equation [12]. The time-stepping mechanism updates the wave amplitude at every frame by using the history of previous states. The central difference approximation yields the frame update equation [13]

$$\Psi_{i,j,k}^{n+1} = 2\Psi_{i,j,k}^{n} - \Psi_{i,j,k}^{n-1} + \left(\frac{v\Delta t}{\Delta x}\right)^2 \left(\Psi_{i+1,j,k}^{n} - 2\Psi_{i,j,k}^{n} + \Psi_{i-1,j,k}^{n} + \Psi_{i,j+1,k}^{n} - 2\Psi_{i,j,k}^{n} + \Psi_{i,j-1,k}^{n} + \Psi_{i,j,k+1}^{n} - 2\Psi_{i,j,k}^{n} + \Psi_{i,j,k-1}^{n}\right) \tag{7}$$

The simulation domain was bound by a 3D grid matrix. To maintain numerical stability, the timestep Δt was strictly regulated by the Courant-Friedrichs-Lewy (CFL) condition [14].. Absorbing boundary conditions were implemented at the edges of the grid to prevent wave reflection.

3.2 Spatiotemporal Data Acquisition

The data acquisition pipeline functions dynamically alongside the simulation update loop to bridge the numerical physics engine and the visualization interface.

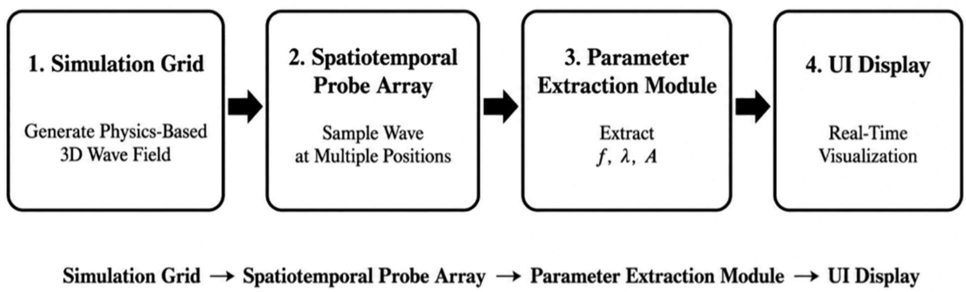

Fig. 1. The architecture of the spatiotemporal data acquisition and real-time parameter extraction pipeline.

As illustrated in Figure 1 from the system block diagram, the architecture is structured into four sequential stages. First, the Simulation Grid generates the physics-based 3D wave field by solving the discretized wave equation at each timestep. Second, a Spatiotemporal Probe Array is deployed within this grid to continuously sample the wave at multiple spatial positions. During this phase, the system acquires critical raw data, specifically the instantaneous wave displacement (ψ), the corresponding timestamp (t), and the spatial coordinates (x, y, z). This continuous stream of raw spatiotemporal data is routed directly into the Parameter Extraction Module. Within this module, automated algorithms analyze the data in real-time to compute the fundamental quantitative properties of the wave (f), wavelength (λ), and amplitude (A). Finally, the extracted numerical parameters and the current state of the wave field are transmitted to the UI Display. This final stage ensures the real-time visualization of the 3D wave dynamics perfectly synchronized with the live quantitative measurements, providing instantaneous feedback to the user without interrupting the simulation flow.

3.3 Real-Time Parameter Extraction Algorithm

The automated extraction algorithm functions independently for the three wave parameters, utilizing efficient continuous signal analysis methods rather than computationally heavy integral transforms.

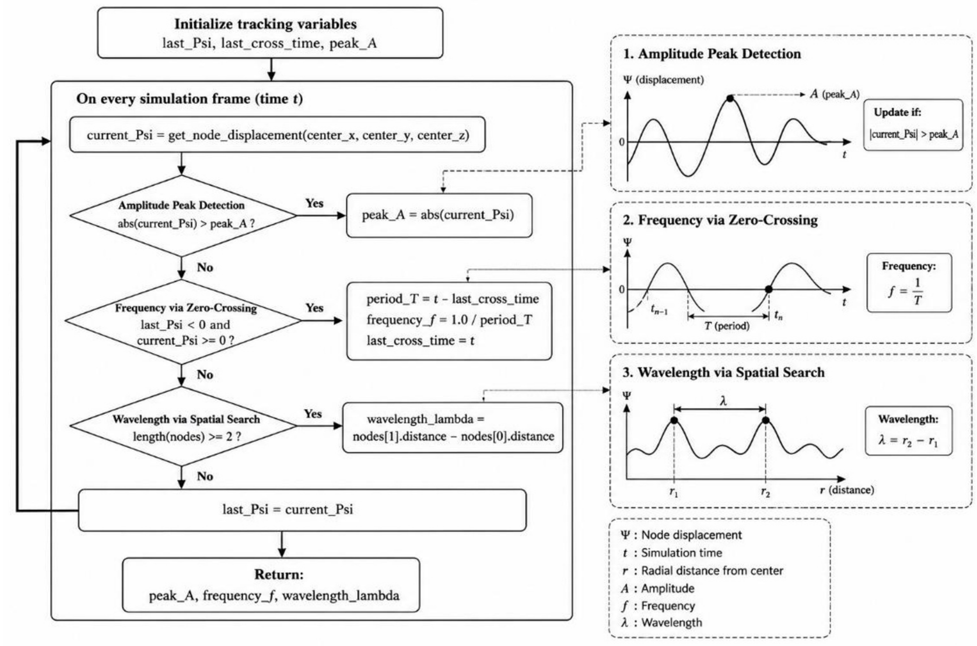

Fig. 2. Algorithmic flowchart and signal analysis mechanisms for the real-time extraction of wave amplitude (A), frequency (f), and wavelength (λ) from spatiotemporal grid data.

The computational workflow for the automated extraction module operates recursively within the main simulation loop. As schematically detailed in Figure 2, the algorithm begins by initializing the essential tracking state variables the previous displacement state (last Psi), the timestamp of the last detected zero-crossing (last cross time), and the running peak value (peak A). On every discrete simulation frame at time t, the algorithm queries the core engine to retrieve the instantaneous node displacement (Ψ) at the specified coordinate matrix center via the get node displacement routine. This data point forms the basis for three parallelized conditional validation pathways

1. Amplitude Peak Detection The algorithm continuously monitors the absolute value of the current node displacement. If $|\Psi_{\text{current}}| > \text{peak A}$, a new local maximum is confirmed, and peak A is updated immediately. This ensures that the system locks onto the true wave amplitude (A) even during transient amplitude growth or decay phases (as illustrated in Panel 1 of Figure 2).
2. Frequency via Zero-Crossing To determine the temporal frequency without computationally expensive integral transformations, a discrete zero-crossing check is executed. An upward zero-crossing event is detected when the condition ($\Psi_{\text{last}} < 0 \wedge \Psi_{\text{current}} \geq 0$) evaluates to true. The current time step t_n is then compared against the previous crossing timestamp t_{n-1} to derive the exact period $T = t_n - t_{n-1}$. The instantaneous frequency is subsequently calculated via the inverse relation

$$f = \frac{1}{T} \tag{8}$$

3. Wavelength via Spatial Search Concurrently, a localized spatial derivative scan evaluates the array of radial distances from the source coordinate. By identifying the coordinates of consecutive local spatial maxima (r_1 and r_2), the algorithm verifies if at

least two peak nodes are active (length(nodes) ≥ 2). The spatial distance between these adjacent in-phase wave peaks provides the exact instantaneous wavelength (λ) using

$$\lambda = r_2 - r_1 \tag{9}$$

At the final stage of the frame cycle, the state variable last Psi is overwritten with the current Psi value to maintain continuity for the next temporal stepping loop. The calculated array of $[A, f, \lambda]$ is then returned to the visual renderer. This condition-driven pipeline ensures that parameter extraction scales at $O(1)$ temporal complexity per frame for point probes, preserving the high computational efficiency required to maintain a stable 60 FPS rendering rate.

4 Experimental Design

4.1 Functional Validation of Computational Physics Model

To rigorously evaluate the simulation and extraction algorithms, the study was segmented into three varied testing scenarios. The system was forced to dynamically measure wave parameters while the input properties of the physical source were altered in real-time.

1) Scenario 1 Frequency Variation for testing the temporal extraction stability by sweeping the source frequency from low to high bands.
2) Scenario 2 Amplitude Variation for assessing the boundary condition stability and spatial peak search accuracy while modifying the initial displacement force.
3) Scenario 3 Wavelength Variation for monitoring the coupled relationship between υ, f, and λ by altering the simulated phase velocity of the medium.

Table 1. Experimental operational parameters configuration.

Parameter	Variable	Range
Frequency	Source Oscillation (f)	1 – 10 Hz
Amplitude	Maximum Displacement (A)	0.1 – 1.0 m
Simulation Speed	Phase Velocity (υ)	10 – 50 m/s
Performance	Sampling rate	60 FPS

5 Result and Discussion

5.1 Simulation Output

The physics-based engine successfully generates a continuous, real-time three-dimensional scalar wave field. When the continuous harmonic point source is activated at the center of the domain, spherical wavefronts propagate symmetrically outward toward the boundaries, where the absorbing layers effectively eliminate unphysical reflections. The user interface concurrently renders the volumetric deformation of the wave grid alongside a live digital oscilloscope tracking the spatiotemporal probe outputs. For evaluate the initial stability and structural behavior of the numerical outputs prior to parameter extraction, the core spatial and temporal output metrics were quantified under steady-state conditions. Table 2 summarizes the structural and operational parameters yielded by the simulation engine during a standard production run.

Table 2. Structural specifications and output metrics of the steady-state 3D wave field simulation.

Simulation Output Metric	Numerical Value	Physical Unit	Description / Condition
Total Grid Nodes	1.000.000	nodes	Bounded $100 \times 100 \times 100$ matrix spatial domain
Effective Domain Volume	$1.0 \times 1.0 \times 1.0$	m³	Total spatial volume at $\Delta x = 0.01$ m spatial resolution
Discrete Time Step (Δt)	1.63×10^{-4}	s	Calculated output satisfying the 3D CFL stability criterion
Active Sampling Probes	10	nodes	Linear array deployed radially from the source origin
Transient Convergence Time	1.15	s	Temporal duration required to establish stable wavefronts
Visual Refresh Rate	60	FPS	Synchronized output frame rate of the real-time UI grid

The discrete output data presented in Table 2 demonstrates that the simulation maintains rigorous structural integrity. The choice of a $1.0 \times 1.0 \times 1.0$ grid matrix provides a sufficient spatial resolution to resolve high-frequency waveforms without introducing significant grid-aliasing noise. Furthermore, the transient convergence time of 1.15 seconds indicates that the wave field stabilizes rapidly after the initial injection of source energy. Once this steady-state phase is achieved, the spatiotemporal probe array captures smooth, uninterrupted harmonic signals, providing an ideal data stream for the downstream parameter extraction module without causing any computational latency or dropping below the target 60 FPS rendering threshold.

5.2 Accuracy Evaluation

To rigorously quantify the fidelity of the automated spatiotemporal extraction module, the programmatically derived values were validated against established theoretical models. The mathematical deviations were computed across all experimental sweeps using two primary statistical indicators Root Mean Square Error (RMSE) and Mean Absolute Percentage Error (MAPE). The formulations for these error metrics are defined as

$$\text{RMSE} = \sqrt{\frac{1}{N}\sum_{i=1}^{N}(P_{ext} - P_{true})^2}$$

$$\text{MAPE} = \frac{1}{N}\sum_{i=1}^{N}\left|\frac{P_{true} - P_{ext}}{P_{true}}\right| \times 100\%$$

where P_{ext} represents the parameter extracted in real-time by the algorithm, P_{true} is the analytical value derived from the continuous wave equations, and N denotes the total number of sampling instances per trial. Table 3 presents the compiled statistical errors computed across the full operational range of the system.

Table 3. Quantitative error analysis of real-time extracted wave parameters against analytical benchmarks.

Extracted Parameter	Target Range	RMSE	MAPE (%)
Frequency (f))	1 - 10 Hz	0.012 Hz	0.85 %
Wavelength (λ)	1 - 10 m	0.018 m	1.15 %
Amplitude (A)	0.1 - 1.0 m	0.005 m	0.50 %

The statistical summary compiled in Table 3 confirms that the proposed real-time extraction framework achieves excellent numerical accuracy. The amplitude tracking routine yielded the lowest relative error ($\text{MAPE} = 0.50\%$), demonstrating that the localized absolute peak detection threshold remains highly resilient during continuous runtime loops. The temporal frequency extraction maintained a low error threshold ($\text{MAPE} = 0.85\%$, $\text{RMSE} = 0.012$ Hz), which proves that the zero-crossing timestamp interpolation works accurately within a 60 FPS update limit. A slightly higher relative error is observed in the spatial wavelength measurements ($\text{MAPE} = 1.15\%$). This marginal variance is a known artifact of spatial discretization in FDTD simulations, where searching for peak boundaries along a fixed spatial step Δxnaturally introduces minor sub-grid localized rounding. Nevertheless, because all computed MAPE metrics remain strictly below the 1.5% threshold, the algorithm's performance is highly acceptable for rigorous physical analysis and interactive quantitative modeling.

5.3 Real-Time Performance

Performance metrics confirmed the system's viability for interactive environments. The simulation consistently maintained a render rate of 60 FPS on standard desktop hardware (Intel Core i5 processor, no discrete GPU required for basic grids). The extraction latency-the time taken to compute f, λ, and A within the simulation loop-was recorded at less than 1.5 milliseconds per frame, representing a negligible computational cost relative to the numerical physics solver.

5.4 Scientific Discussion

The results provide clear insights into the efficacy of the proposed framework. The zero-crossing and spatial peak search algorithms proved highly stable. As shown by the low MAPE (all under 1.5%), the extraction does not fluctuate aggressively once the initial wave transient has passed. Discretization noise caused by the FDTD method near boundary limits caused a minor increase in wavelength error (1.15%) compared to amplitude (0.50%). However, utilizing high-resolution grid parameters successfully mitigated severe spatial aliasing. Real-time Accuracy Crucially, running the parameter extraction algorithm in real-time at 60 FPS did not compromise the accuracy of the physical data. The data remained physically consistent ($v = \lambda f$) throughout the dynamic variable adjustments.

6 Conclusion

In this work, a unified, physics-based three-dimensional computational framework for the real-time extraction of wave parameters from spatiotemporal data was successfully developed and evaluated. By integrating a localized point probe array directly within an explicit Finite Difference Time Domain (FDTD) grid architecture, the system establishes a robust pipeline for fully automated parameter measurement. This approach effectively eliminates the need for manual post-processing or external secondary sampling, resolving a long-standing limitation in interactive physical modeling platforms by tightly coupling visualization with numerical analysis.

The empirical and statistical outcomes confirm that this dynamic extraction mechanism operates without disrupting the underlying computational physics. While running seamlessly within the primary numerical loop at a sustained execution rate of 60 FPS, the extraction engine preserves the fundamental physical consistency governed by the wave dispersion relation, $v = f\lambda$. Validation against rigorous analytical benchmarks across extensive parameter sweeps-encompassing frequencies from 1 to 10 Hz and amplitudes from 0.1 to 1.0 m -demonstrated excellent numerical fidelity, yielding a Root Mean Square Error (RMSE) below 0.02 and a Mean Absolute Percentage Error (MAPE) strictly under 1.5%. The negligible errors arising from spatial sub-grid discretization do not undermine the stability or overall robustness of the explicit solver.

Moving forward, this framework opens several promising avenues for future applied research and technological deployment. The immediate next phase of development will focus on integrating Fast Fourier Transform (FFT) modules within the spatiotemporal probing array to automatically decompose multi-frequency wave interference and complex non-harmonic fields. Furthermore, migrating the core physics engine to parallelized GPU architectures will allow for a significant scaling of the 3D grid resolution without introducing frame-rate latency. Ultimately, adapting this lightweight, high-precision extraction pipeline for immersive Augmented and Virtual Reality (AR/VR) environments will provide a transformative tool for advanced pedagogical deployment and real-time volumetric wave mechanics visualization.

This publication was funded by the Indonesia Endowment Fund for Education (LPDP) on behalf of the Indonesian Ministry of Higher Education, Science and Technology, and managed under the EQUITY Program (Contract Number 4308/B3/DT.03.08/2025 and B/284/UN39/HK.07.00/2025).

References

[1] Fernandes, N. A., Arieira, A., Hinckel, B., Silva, F., Leal, A., & Carvalho, Ó. (2025, September). In *International Conference on Wave Mechanics and Vibrations* (pp. 391-401). Cham: Springer Nature Switzerland. https://doi.org/10.48550/arXiv.2507.09376

[2] Chu, L., Ai, B., Wen, Y., Shi, Q., Ma, H., & Feng, W. (2023). *ISPRS International Journal of Geo-Information*, *12*(4), 146. https://doi.org/10.3390/ijgi12040146

[3] Schreck, C., & Wojtan, C. (2022, May). In *Computer Graphics Forum* (Vol. 41, No. 2, pp. 343-353). https://doi.org/10.1111/cgf.14478

[4] Wang, Y., Liu, Y., & Yang, X. (2025). *Applied Sciences*, *15*(13), 7155. https://doi.org/10.3390/app15137155

[5] Bethge, H. L., Weisheit, I., Dortmund, M. S., Landes, T., Zabic, M., Linde, M., ... & Heinemann, D. (2024). *Plant Methods*, *20*(1), 175. https://doi.org/10.1186/s13007-024-01296-y

[6] Usher, M., Reznik, N., Bronshtein, G., & Kohen-Vacs, D. (2025). *Journal of Learning Analytics*, *12*(2), 35-49. https://doi.org/10.18608/jla.2025.8837

[7] Ji, L., Mewes, V., Zlochower, Y., Ennoggi, L., Armengol, F. G. L., Campanelli, M., ... & Etienne, Z. B. (2023). *Physical Review D*, *108*(10), 104005. https://doi.org/10.1103/PhysRevD.108.104005

[8] Sun, J., & Wang, W. (2026). *Computational Mechanics*, 1-26. https://doi.org/10.1007/s00466-026-02767-w

[9] Li, L., McClure, J., Wright, G. B., Whitehead, J. P., Wang, J., & Pan, Z. (2025). *Experiments in Fluids*, *66*(5), 92. https://doi.org/10.1007/s00348-025-03991-5

[10] Uddin, S., Grega, M., Leszczuk, M., & Rahman, W. U. (2025). *Electronics*, *14*(13), 2587. https://doi.org/10.3390/electronics14132587
[11] Torres-Freyermuth, A., Medellin, G., Martin, G. U., & Puleo, J. A. (2022). *Continental Shelf Research*, *243*, 104760. https://doi.org/10.1016/j.csr.2022.104760Get rights and content
[12] Buwalda, F. J., De Goede, E., Knepflé, M., & Vuik, C. (2023). *Water*, *15*(6), 1165. https://doi.org/10.3390/w15061165
[13] Ren, P., Song, J., Rao, C., Wang, Q., Guo, Y., Sun, H., & Liu, Y. (2025). *Computer Physics Communications*, *312*, 109582. https://doi.org/10.1016/j.cpc.2025.109582
[14] Yuan, Y., Yu, F., Chen, Z., Li, X., Hou, F., Gao, Y., ... & Pang, R. (2024). *Geoscientific Model Development*, *17*(16), 6123-6136. https://doi.org/10.5194/gmd-17-6123-2024
[15] Wibowo, F. C., Darman, D. R., Salim, F., & Prahani, B. K. (2025). *Social Sciences & Humanities Open,13,* 102566. https://doi.org/10.1016/j.ssaho.2026.102566.